

Chapter 8

Polymer/Graphene Composites for Energy Storage

Yuchen Liu and Shiren Wang

Abstract In recent years, tremendous research effort has been focused on novel supercapacitors because of their stable ultra-high power density, cycling life, and fast charging–discharging rate. These researches aimed at increasing the energy density of supercapacitors without sacrificing high power capability so that they reach the levels achieved in batteries and at lowering fabrication costs. For this purpose, conjugated polymers have been effectively integrated with graphene nanosheets for supercapacitor applications, which sparked great excitement in superior performance owing to their synergistic effects on charge absorption and transportation, and extraordinary characteristic of the reversible oxidation–reduction activity which enables a high energy density. In this chapter, simple pathways to tailor polymer/graphene composites architectures for improving supercapacitor performances were summarized. Further, a theoretical model has been established to quantify the influences of various factors on the supercapacitor behaviors. On this basis, challenges and perspectives in this exciting field are also discussed. These results not only provide fundamental insight into supercapacitors but also offer an important guideline for future design of advanced next-generation supercapacitors for industrial and consumer applications.

8.1 Introduction

With the rapid growth of hybrid vehicles and renewable energy systems, there is an urgent need for developing advanced electric energy storage with high-storage capacity and fast charge–discharge ability to meet practical application [1]. Among available energy storage devices, there are three typical traditional energy storage devices: fuel cells, batteries, and capacitors. Fuel cells have the largest energy density, while capacitors have the highest power density. The energy and power

Y. Liu · S. Wang (✉)

Department of Industrial and Systems Engineering, Texas A&M University,
College Station, TX 77843, USA
e-mail: S.Wang@tamu.edu

© Springer International Publishing AG 2017

Z. Lin et al. (eds.), *Polymer-Engineered Nanostructures for Advanced
Energy Applications*, Engineering Materials and Processes,
DOI 10.1007/978-3-319-57003-7_8

337

density of lithium batteries are between fuel cells and capacitors. Supercapacitors were invented in 1970s and quickly became one of the rising stars in the new century. Supercapacitors are a type of energy storage whose power density is extremely high compared with traditional batteries [2]. Physical, rather than chemical, energy storage makes it possible to operate safely and extend the life cycle. As the superior performance on the rate of charging and discharging, supercapacitor can be applied in electric vehicles (EV) [3]. From the comparison of all the devices presented above, the applications of supercapacitors are hindered by low energy density. Although supercapacitors have a much larger energy density than traditional capacitors, they have far less energy density than lithium batteries [4–6]. That is why supercapacitors are always installed with lithium batteries as a power device. In order to solve this challenge, high-performance supercapacitor with high energy density is needed to be developed. Graphene is selected as a promising material for various energy systems such as supercapacitors, solar cells, and fuel cells because of its reversible oxidation–reduction activity and the good conductivity of graphene. Hence, graphene materials are always composited with polymers which can promote the process ability and/or flexibility of graphene materials [7].

There are two types of supercapacitors according to the different charging–discharging mechanisms. The first one, performed from a double-layer capacitance, is called (electric or) electrochemical double-layer capacitor (EDLC). And the other one is so-called faradic pseudo-capacitor [8]. The definition of the capacitance of the EDLC is shown as below:

$$C_s = \frac{A\epsilon_0\epsilon_r}{d}, \quad (8.1)$$

where C_s is the specific capacitance, ϵ_0 is the vacuum dielectric constant, and ϵ_r is the dielectric constant of electrolyte, A is the effective surface area, and d is the effective thickness of the electric double layer. This equation guides the direction of increasing the capacitance of EDLCs. EDLC materials always have a large effective surface area of the electrodes. Compared with the traditional physical capacitors, the thickness of the electric double layer (which refers as d in Eq. 8.1) varies within several nanometers, resulting in a larger specific capacitance.

The basic structure of an EDLC is shown in Fig. 8.1a. The membrane only allows ions to pass through in order to avoid the short circuit. During the charging process, the ions move to the opposite charged electrode and attach onto the electrode via electrostatic attraction. During the discharging process, the electrons travel through the external circuit, the ions leave the electrodes and consequently the system goes back to neutral. The structure of EDLC gives it huge power density because of extremely high-speed absorption/desorption process between thin electrochemical double layer and consequently resulting in the steady charge and discharge throughout a wide charge–discharge rate as shown in Fig. 8.1b.

On the other hand, the mechanism of the faradic pseudo-capacitor is more complicated than EDLC. Besides the huge surface area like that of EDLC, it also

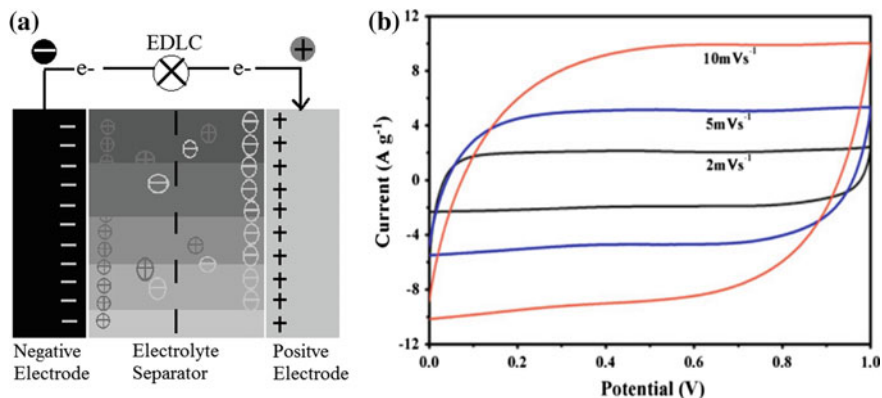


Fig. 8.1 Typical structure of EDLCs (a); representative cyclic voltammogram of EDLC (b) (Reproduced from Ref. [2] with kind permission of © 2004 American Chemical Society, and Ref. [5] with kind permission of © 2010 Springer)

involves the reversible electrochemical reactions. The definition of the capacitance of the pseudo-capacitor is shown as below:

$$i_p = an^{1.5}AD^{0.5}Cv^{0.5} \quad (8.2)$$

$$i = i_p \frac{nF}{RT} (E - E_{eq}) \quad (8.3)$$

$$C_s = \frac{\int idt}{\Delta Vm}, \quad (8.4)$$

where i_p stands for peak current of electrode when electrochemical reactions occur, a is a constant number of 2.69×10^5 , n is the number of electrons transferred in a specific electrochemical reaction, A is the effective surface area of electrode, D is the diffusion coefficient of electrolyte, v is the scan rate, C is the bulk concentration of electrolyte, t is the scanning time during the test, ΔV is the voltage difference between the beginning and of the end of scan, m is the mass of the electrode, i is the electrode current, F is the Faraday's constant, R is gas constant, T is thermodynamic temperature, E is the on-site potential, E_{eq} is the standard electrode potential for an electrode/electrolyte combination, and C_s is specific capacitance.

It is easy to realize that the specific capacitance of the pseudo-capacitor is determined by many variables. The peak value depends on the number of electrons transferred during the electrochemical reaction and the intrinsic property of the electrode material. The second most significant factor is the efficient surface area, and the third one is the diffusion coefficient of ions in the electrolyte. Hence, increasing the effective surface area, electrolyte concentration, and electrolyte diffusion coefficient is the key direction in enhancing the capacitance of pseudo-capacitor, after the electrode material is selected. The basic structure and

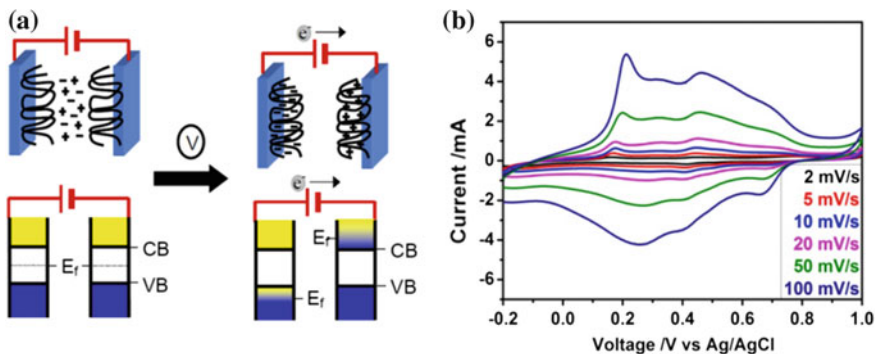


Fig. 8.2 Typical structure of pseudo-capacitor (a); representative cyclic voltammogram of pseudo-capacitor (b) (Reproduced from Ref. [4] with kind permission of © 2004 SERDP)

cyclic voltammetry of pseudo-capacitors are presented in Fig. 8.2. The majority of difference between the EDLC and the pseudo-capacitor is that the materials of the pseudo-capacitor which have two or more reversible oxidation states (shown in Fig. 8.2a). During the charging process, the electrode received the charges from the ions and transferred to a higher oxidation state. The electric energy is transferred and stored as chemical energy. During the discharging process, the electrons move from the negative electrode to the positive one via the external loop, and electrode loses charges and goes back to the base state.

There are three main methods to determine the capacitance of conducting polymer materials, namely, constant current charge–discharge, cyclic voltammetry (CV), and electrochemical impedance spectroscopy (EIS). Theoretically, the charge–discharge curve for a capacitor should be linear with a slope equal to the current divided by the capacitance. Without the influence of redox processes, the cyclic voltammogram of a capacitor would be shaped as rectangular and the capacitance is equal to half the value of difference in plateau currents divided by the scan rate. The slope of the EIS data can represent the capacitance of a capacitor.

8.2 Polymer/Graphene Composite

8.2.1 Electrode Material Selection

8.2.1.1 Carbon-Based Materials

Most EDLC is based on the carbon materials which have huge surface areas and good electrical conductivity. In the ideal EDLCs, the only possible reaction which can reduce the life cycle of the materials is electrostatic attraction. High rate of charging–discharging in EDLC also refers to high power density. Hence, the main

research about EDLC focuses on improving the energy density and specific capacitance. In order to improve the capacitance, according to Eq. (8.1), it is effective to enlarge the effective surface area of electrode materials. Meryl D. Stoller et al., firstly, used chemically modified graphene (CMG) as the EDLC electrode material. The surface area measured by Brunauer–Emmett–Teller (BET) method was 705 m²/g. And the specific capacitance was calculated as 135 and 99 F/g in aqueous and organic electrolyte, respectively, which are much lower than the theoretical value, 550 F/G [6]. Yoo et al. applied chemical vapor deposition to fabricate the ultrathin “planar graphene” and used a perpendicular electrode to avoid the agglomeration of graphene which commonly happened in the chemically prepared graphene. As a result, the surface area of planar graphene was significantly increased as high as 1310 m²/g, and the specific capacitance can reach 247 F/g [9].

Kaner et al. employed laser scribed graphene (LSG) film as the electrode of supercapacitor. LSG can increase the surface area as 1520 m²/g, and hence the capacitance can reach 276 F/g [10]. Another research reported by Zhu et al. increased the effective surface area of graphene up to 3100 m²/g by via the chemical activation of microwave (or thermally)-exfoliated GO [11]. The recent trend focuses on PANI/graphene supercapacitor. Xie et al. demonstrated that the wavy-shaped PANI/graphene-based supercapacitor can reach 261 F/g capacitance and an energy density of 23.2 Wh/kg at a power density of 399 W/kg for a 0.8 V voltage window. Based on the above research, the theoretical capacitance of 550 F/g is difficult to achieve because the surface area of single-layer graphene is not fully used for charge transition at the electrochemical double layer. Although, it is hard to increase the specific capacitance of carbon-based materials, and the energy density is readily increased according to the equation:

$$E = \frac{1}{2} C_s V^2, \quad (8.5)$$

where E is energy density, C_s is the specific capacitance, and V is the voltage difference between the beginning and the end of discharging. Graphene is a relatively inert material even at high voltage. As a result, it is easy to increase energy density by adding the voltage. Water will electrolysis at 1.22 V, and it is easy to overcome this problem with replacing water by other organic electrolyte. EMIMBF₄ ionic liquid electrolyte can hold 4 V, which brought 16 times increments compared with water [3, 12]. Other organic systems were also studied, such as TEABF₄/PC, TEABF₄/AN [6, 13, 14], NEt₄BF₄-PC [15, 16], LiClO₄/PC [17], and BMIM BF₄/AN [11].

8.2.1.2 Conducting Polymer Materials

On the other hand, there are two main types of pseudo materials: metal oxides and conjugated polymers. The stored energy in these materials can be also classified into two types: direct electrostatic attraction and reversible chemical–electrical

energy conversions. Hence, a pseudo-capacitor can store much more energy and thus has a larger energy density at same voltage range. During charge–discharge process, negative ions can diffuse through the crystals of metal oxides and form metal complexes. Because of the robust structure of the crystal, the metal oxide to metal complex transition is highly reversible. This could result in long cycling life close to EDLCs. McKeown et al. used RuO_2 as pseudo materials which can make the specific capacitance reach the theoretical value 720 F/g.

Most recently, conjugated polymers have been investigated as electrode materials because of their fast kinetics of charge/discharge, high electrical conductivity, mechanical flexibility, and low cost [18]. Conducting polymers are easily to be manufactured as self-supporting, flexible thin film. These advantages attracted researchers as an ideal electrode material for flexible supercapacitor applications. However, the durability and electrochemical stability must be considered because of the stresses during charge/discharge process. Polyaniline (PANI), polypyrrole (PPy), polythiophene (PT), and PEDOT, and composites containing them are widely considered as electrode materials (Table 8.1).

Table 8.1 Specific capacitances of composite and treated materials [8]

Electrode material	Specific capacitance (F/g)	Electrolyte
PPy-SWNTs	144	Aqueous
PPy-funct-SWNTs	200	Aqueous
PEDOT-on-PPy	230	1 M LiClO_4 (aq)
PEDOT-on-PPy	290	1 M KCl (aq)
PPy- Fe_2O_3	420	LiClO_4 (aq)
PPy	78–137	PVDF-HFD gel electrolyte
PEDOT- MoO_3	300	Nonaqueous Li^+
Nonirradiated HCl-doped PANI	259	Gel polymer electrolyte
Nonirradiated HCl-doped PANI	210 (10,000 cycles)	Gel polymer electrolyte
Irradiated HCl-doped PANI	243	Gel polymer electrolyte
Irradiated HCl-doped PANI	220 (10,000 cycles)	Gel polymer electrolyte
RuOX-PEDOT-PSS	1409	
PPy-fast CV deposited	480	1 M KCl (aq)
ACP-PANI	273	1 M H_2SO_4
Non-treated PEDOT	72	1 M H_2SO_4
Ultrasonicated synthesis of PEDOT	100	1 M H_2SO_4
MWNT/PANI 20/80 wt%	360	
MWNT/PPy 20/80 wt%	190	
PANI coated CNF (20 nm)	264	
PEDOT/MSP-20	56 (1000 cycles)	Et_4NBF_4 in PC, LiPF_6 in EC/DMC

Polyaniline

PANI is considered one of the most promising supercapacitor or battery electrode material because of its low cost, ease of synthesis, high theoretical capacity, flexibility, high conductivity, good redox reversibility, and environmental stability [19–39]. The theoretical specific capacitance of PANI is 2000 F/g (if PANI is fully oxidized or reduced in charging–discharging process) [40]. However, a major constraint of PANI is that it needs a proton to be properly charged and discharged; as a result, a protic solvent, an acidic solution, or a protic ionic liquid is required [29]. The specific capacitance is higher for electrodeposited formed PANI than for chemically formed one. The capacity of PANI is varied from 44 to 270 mAh/g [19]. This variation comes from many factors, including synthetic route used, polymer morphology, the amount and type of binders and additives, and the thickness of the electrode. It is a good idea to use the method of design of experiment (DOE) to figure out the most significant factors.

To maximize capacitive behavior, the morphology of the PANI can be controlled on the nanoscale by forming nanowire or nanofibers. In the literature, Zhao et al. reported the highest specific capacitance as 1142 F/g when PANI nanowire was prepared by electrodeposition on an anodic aluminum oxide (AAO) template [41]. The fibrous PANIs were published owing higher effective surface area than those of non-fibrous PANI [42, 43]. The specific capacitance of thin nanofibrous PANI was 160 F/g, which is higher than that of thick nanofibrous PANI or that of spherical (non-fibrous) PANI for 120 and 90 F/g, respectively. The surface area measured by Brunauer–Emmett–Teller (BET) method was 70 m²/g for the thin PANI nanofibers which is much larger for thick PANIs or spherical PANIs for 21 or 13 m²/g, respectively.

Polypyrrole

PPy is another promising supercapacitor electrode material which offers a great degree of flexibility [44–67]. PPy is typically doped with single-charged anions such as Cl[−], ClO₄[−], and SO₃. But if doped with multiple-charged anions, e.g., SO₄^{2−}, physical cross-linking of the polymer occurs [68]. The theoretical specific capacitance of PPy is 620 F/g [69]. The supercapacitors which were assembled by poly-vinylidene fluoride *co*-hexafluoropropylene (PVDF-HFP)-based gel electrolytes sandwiched between PPy electrodes showed the specific capacitances about 78–138 F/g [70]. Other researchers demonstrated PPy-Nafion deposited on Pt or PPy modified composited membranes with good specific capacitance and cyclic stability for electrochemical applications [71, 72]. PPy/Nafion and PPy/paratoluene sulfonated, decomposited onto a gold-coated polyvinylidene difluoride (PVDF) membraned substrate, showed specific capacitances of 380 and 430 F/g, respectively. The PPy/Nafion electrode showed better properties on the cycling life and energy density than that of the PPy/paratoluene sulfonate electrode. In the CV curves, the capacitance of PPy/Nafion electrode was conserved up to 70% after 5000

cycles, whereas the capacitance of PPy/paratoluene sulfonate was only 12% remaining.

On the other hand, PPy nanospheres were able to be prepared in graphene layers to form a three-dimensional hierarchical cross-linking structure through simple hydrothermal method [73]. Gan et al. built a symmetric supercapacitor from the porous MnO_2/PPy nanocomposite yielded a specific capacitance of 142 F/g per mass of one electrode. The cycling life of this capacitor remained 93.2% capacitance retention after 1000 cycles [74].

Polythiophene

The electrical conductivity and the theoretical capacitance of polythiophene are estimated to be 300–400 S/cm and 485 F/g, respectively. In the literature, the specific capacitances of polythiophene derivatives showed as about 220 F/g [75]. Although this capacitance is lower than that of PANI and PPy, poly(3,4-ethylenedioxy-thiophene) (PEDOT) has advantages due to chemical and thermal stability in the oxidized form and fast electrochemical switching [76, 77]. PEDOT has many advantages such as good electrical conductivity, flexibility, low cost, and pseudo-capacitance. PEDOT was used as an active material in supercapacitors. In the recent research, the processing temperature of vapor phase polymerization (VPP) showed a significant effect on PEDOT morphology, the degree of orientation, and its electrical properties. By this effect, PEDOT-based composites show a specific capacitance up to 134 F/g with the polymerization temperature of 110 °C [78]. Zhao et al. used binder-free porous PEDOT electrodes for flexible capacitors. The specific capacitance, energy density, and coulombic efficiency of the PEDOT supercapacitor can reach 69 F/g, 24 Wh/kg, and 95% at a current density of 0.2 A/g, respectively. Also, PEDOT electrodes presented good cycling performance. The capacitance retention ratio is about ~72% after 1500 cycles. The results of PEDOT film from different current densities and scanning rates show the supercapacitors have better rate performances [79].

The use of PEDOT nanowires enables assembly of PEDOT mats which can be assembled into all-textile flexible supercapacitors using carbon cloth as the current collector. Electrospun polyacrylonitrile (PAN) nanofibrous membranes were used as the separator. Ionic liquid-impregnated PVDF-co-HFP was used as the solid electrolyte. The specific capacitance was shown about 20 F/g [80].

8.2.2 Electrolytes

In supercapacitor, the electrolytes are another significant part need to be considered. In common, the charges of a supercapacitor are carried by ions that travel through the electrolyte. Thus, the viscosity, ionic conductivity, and boiling points of

electrolytes are all key factors. Generally, electrolytes can be divided into three types: aqueous electrolyte, ionic liquid, and solid-state electrolyte.

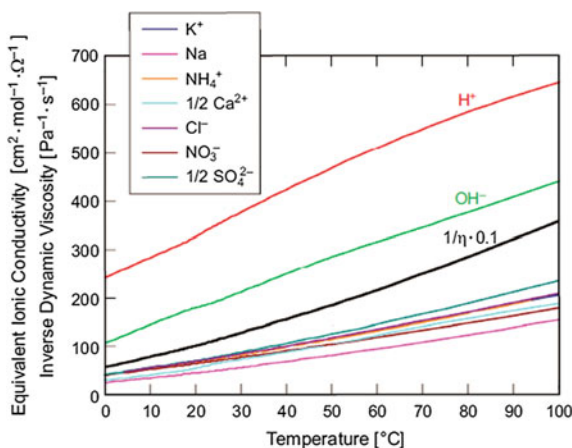
8.2.2.1 Aqueous-Based Electrolytes

Aqueous-based electrolytes, which have low price, compatibility with most salts, and high ionic conductivity, are extensively investigated and widely used. The conductivity of aqueous electrolyte can be calculated in the following equation [81]:

$$\kappa = \sum C_i Z_i \lambda_i, \quad (8.6)$$

where C_i is the concentration of dissolved ion i , Z_i is the absolute value of the charge number of ion i , and λ_i is the equivalent ionic conductivity of ion i . The measured value of the ionic conductivity of 1 M HCl at room temperature is about 0.347 S/cm. As the HCl concentration and temperature increased, the conductivity increases, respectively [82]. The conductivity of Na_2SO_4 solution is higher than that of HCL, at 4.24 S/cm in 0.5 M at room temperature [83]. However, the application of aqueous electrolytes is limited since the water will be decomposed above 1.22 V. In the literature, the charge–discharge voltage of most aqueous-based supercapacitors is about 0.7–0.8 V. In this situation, the potential of electrodes is far from fully explored [84]. Wagner et al. showed that the equivalent conductivity of various aqueous-based electrolytes increases linearly as the temperature is increased between 0 and 100 °C, and the result can be seen in Fig. 8.3 [81]. As the saturated vapor pressure is relatively high (1 atm at 100 °C), it makes water easy to evaporate and even boil and consequently constraint the application of aqueous-based electrolytes.

Fig. 8.3 Conductivity–temperature dependence of various aqueous electrolytes (Reproduced from Ref. [81] with kind permission of © 2012 Research Gate)



8.2.2.2 Ionic Liquid-Based Electrolytes

Ionic liquid is another major type of the electrolytes which attracted a huge amount of attention for several years. Typically, they kept in the liquid state and ionized organic salts at ambient temperature which results in showing a high ionic conductivity. The detailed chemical structures of cations and anions are presented in Fig. 8.4 [85]. Most of the cations are nitrogen-based hexagons and pentagons in a conjugated structure. As the molecules are stable of the rigid and conjugated structures, they are more stable in a wide temperature and voltage window, specifically up to 7 V and from -40 to 200 °C. In order to improve the specific capacitance, energy density and power density are directly correlated with charge–discharge voltage, and consequently it is significant to enhance the voltage of the electrochemical performance in a safe manner.

The low ionic conductivity is the key factor of ionic liquid, and it can be expressed by the equation [86]:

$$\Lambda = \frac{e^2 N_A}{k_B T} (D^+ + D^-), \quad (8.7)$$

where Λ is the conductivity at low ion concentration, N_A is Avogadro's number, e is the charge of one electron, k_B is Boltzmann's constant, and D^+ and D^- are the diffusion coefficients of cation and anion, respectively. The correlation between diffusion coefficient and viscosity is quantified by the Stokes–Einstein equation [87]:

$$D = \frac{k_B T}{6\pi\eta r}, \quad (8.8)$$

where η is the viscosity of the ionic liquid and r is the radius of ions. The relationship between viscosity and temperature can be described by Vogel–Fulcher–Tamman equation as followed [88]:

$$\eta = \frac{\eta_0}{T^{\frac{2}{3}}} \exp\left(\frac{B}{T - T_0}\right), \quad (8.9)$$

where η_0 is a pre-exponential constant proportional to the viscosity coefficient, B is the pseudo-activation energy for viscous behavior, and T_0 is the ideal melting temperature of ionic liquid. From the equations, it can be seen that ionic liquids show better features at higher temperature with lower viscosity. On the other hand, a large ion radius results in a small diffusion coefficient and finally a low conductivity. This results in a smaller power density than that of aqueous electrolyte. Compared with other electrolytes, ionic liquids have high cost and lack of physical property and toxicity data which restricting the properly use as process chemicals and processing aids at current state [89]. In addition, as those ionic liquids are still

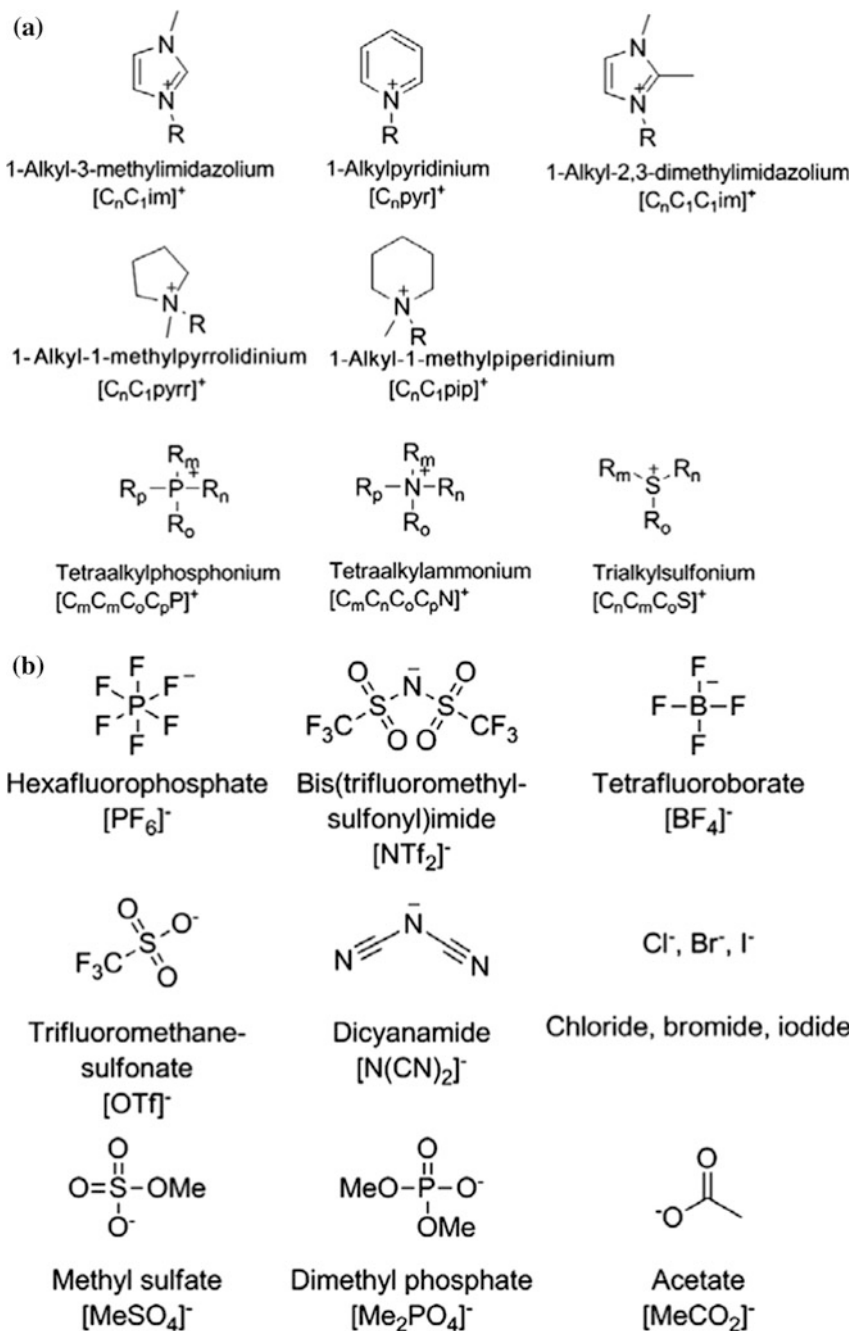


Fig. 8.4 Common ionic liquids: cations (a); anions (b) (Reproduced from Ref. [85] with kind permission of © 2012 Royal Society of Chemistry)

free to flow, a good container and good sealing is required when assembling the products which constrain their applications in flexible supercapacitors.

8.2.2.3 Solid-State Electrolytes

Modern electronics require not only higher and higher energy storage devices, but also other features, such as flexibility, smaller size, safety, and cheaper price. Solid-state electrolyte is the most outstanding candidate to meet all of the requirements. There are mainly two categories of solid-state electrolytes. The first type is glass and ceramics consist of mixture of lithium salts, such as lithium nitrides, sulfides, borates, phosphates, etc. [90–93]. However, most lithium salts are sensitive to moistures and no longer flexible after sintering. Another type of the solid-state electrolyte is the polymer-based solid-state electrolyte, which is prepared by doping proton acids or ionic liquids into polymer matrixes. Polyvinylidene fluoride (PVDF), polyethylene glycol (PEO or PEG), and polyvinyl alcohol (PVA) are the three most employed matrixes. PVDF matrix is coupled with ionic liquids and lithium salts by mixing in organic solvents [94]. PEG and PVA can be coupled with proton acids by dissolving in water making them more commonly used in both in research and applications. Capiglia et al. found that the ionic conductivity of the SiO₂-doped PEO₈-LiClO₄ was about 10⁻⁴ S/cm [95]. In Haijun Yu's study, the conductivity of KI-doped PVA-KOH can reach 10⁻² S/cm [96]. The ionic conductivity of various solid-state electrolytes (and ionic liquids as well) is summarized in the Fig. 8.5 [97]. From the figure, it can be found that the ionic conductivity of PEO-LiClO₄ and LiPF₆/PVDF-HFP systems is only about 10⁻³ S/cm at room temperature. Although they can continuously increase as the increase of the temperature, respectively, their highest values are still only about 10⁻² S/cm at 100 °C which is onefold lower than that of ionic liquid LiBF₄/EMIBF₄ (up to 10⁻¹ S/cm), and twofolds lower than that of aqueous electrolytes. Hence, much lower power density could be expected according to $P = U/(4ESR^2)$. In this situation, low ionic conductivity is the major contributor of ESR.

Although the solid-state electrolytes are widely applied in electronics, the highest ionic conductivity is still lower than that of medium value in proton acids' aqueous electrolyte. Since there is no universal model to describe the conducting mechanism of solid-state electrolytes, the conducting behaviors of solid-state electrolytes can be approximately described by basic semiconductor equations as follows:

$$\sigma = qn\mu. \quad (8.10)$$

This is a universal equation to describe the conductivity of doped semiconductor, where σ is the conductivity, q is the charge of a carrier which is equal to Z^*

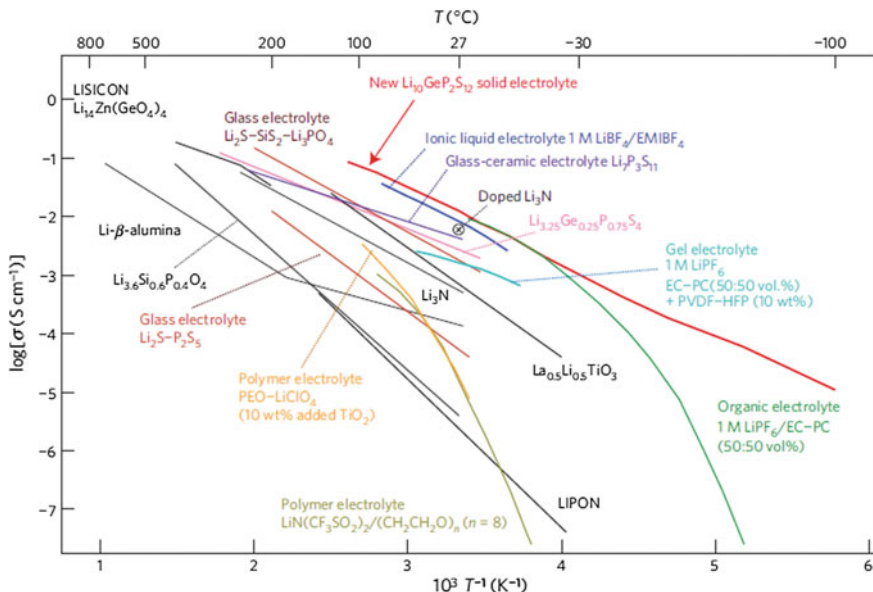


Fig. 8.5 Ionic conductivities of various solid state electrolytes (Reproduced from Ref. [97] with kind permission of © 2011 Macmillan Publishers Ltd)

1.602×10^{-19} C (when carrier is not electron), n is the carrier concentration, and μ is the carrier mobility. The carrier concentration and mobility have different formations depending on different materials.

In organic semiconductors, carrier mobility follows Langevin theory [98]:

$$\mu = \frac{eD}{k_B T}. \tag{8.11}$$

And the carrier concentration can be calculated by following equation [99]:

$$n^{+/-} = \frac{N_A}{1 + g \times \exp((E_A - E_F) / kT)}, \tag{8.12}$$

where N_A is the nominal concentration of dopant, E_A is the ionization energy, E_F is the Fermi energy, g is the degeneracy factor for acceptor levels, and a value of 4 is commonly assigned to g .

It can be seen that the major variable affecting the carrier mobility is the diffusion coefficient. However, Eq. (8.8) is not applicable in the solid. Increasing the dopant concentration is the most direct approach to increase the carrier concentration.

8.3 Preparation of PANI Nanowires/Graphene Composites

In this chapter, three novel, facile, and scalable approaches are presented to control the geometries and structures of the graphene interlinked aligned PANI nanofibers to achieve optimal supercapacitive performance. By carefully selecting the synthesis approaches and parameters, PANI nanofibers with uniform alignment and narrow size distribution are realized. Also, a theoretical model has been established to quantify the electrode structures and performance relationship and to provide the guideline for the future fabrication and optimization. Thus, this chapter provided both experimental and theoretical approaches for constructing high energy density and high power density supercapacitors.

8.3.1 Melamine-Assisted Synthesis of PANI/Graphene Composites

Due to the strong π - π conjugation between the PANI hexagon ring and graphene, it is hard for the PANI to nucleate directly on graphene. Another problem is that graphene sheets and PANI nanowires are usually randomly dispersed and lacked of ordering and porous structure in the hybrids, which can significantly affect the performance of their supercapacitors. Thus, template-assisted nucleation is urgently needed for producing tailored PANI nanowire morphology to meet specified characteristics, such as orientation, size, and distribution. However, it is very challenging to apply a template to various graphene nanosheets randomly dispersed in the colloidal suspension.

In Wang's work [100], a small molecule is reported to generate heterogeneous nucleation of PANI on the graphene sheets to reduce the thickness of the PANI coating. Melamine is a conjugated small molecule, and its molecular structure is shown in Fig. 8.6. Because of the strong π - π conjugate between hexagonal rings, it can be strongly absorbed onto graphene by non-covalent interactions serving as nucleation sites for PANI nanowires. Along with the APS added, the amino groups are dissociated in the acidic solution and initialized the polymerization of PANI. The dilute ANI monomers are used to ensure the subsequent growth of PANI

Fig. 8.6 Structure of melamine

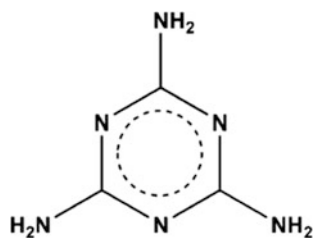
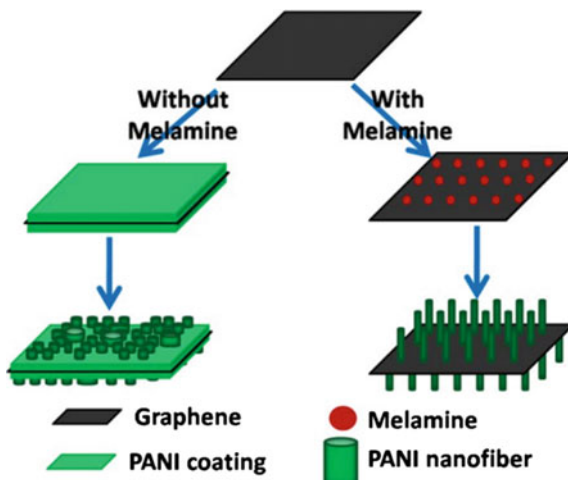


Fig. 8.7 Proposed mechanism of PANI nanowires: growth without melamine and heterogeneous nucleation and growth in bulk solution (Reproduced from Ref. [100] with kind permission of © 2013 Informa Group plc)



nanowires is vertically aligned. The relevant growth mechanism of PANI nanowires is described below (Fig. 8.7).

Simultaneously, melamine is further employed to tune the diameter and area density of PANI nanowires on both sides of graphene sheets by adjusting the concentrations of melamine and ANI. The smallest diameter and largest area density can be achieved when the concentration of melamine is 0.06 mM and ANI is 3 mM. The ordered porous network in the graphene/PANI nanowire hybrids can facilitate the ion diffusion, transportation, and exchange. These results suggest that melamine is promising to design and synthesize tunable nanostructures to meet the various needs.

8.3.2 Graphene Film Cross-Linked Ordered PANI

In Sect. 8.3.1, a soft template directed PANI/graphene hybrid is fabricated in the colloid. Despite its easy preparation and high yield, a lack of processibility is the major challenge in the electrode applications. Also, additional conductive and adhesive materials have to be used to bind the PANI/graphene powders, which will reduce conductivity. To solve these problems, in situ synthesis of a PANI nanowires array on the conductive substrate is more attractive due to the low contact resistance between electrode and current collector. Moreover, the desired structure can be very stable (Fig. 8.8).

In this situation, a multilayered vertically aligned PANI nanowire arrays were prepared by using graphene film as an interlayer [101]. Specifically, the

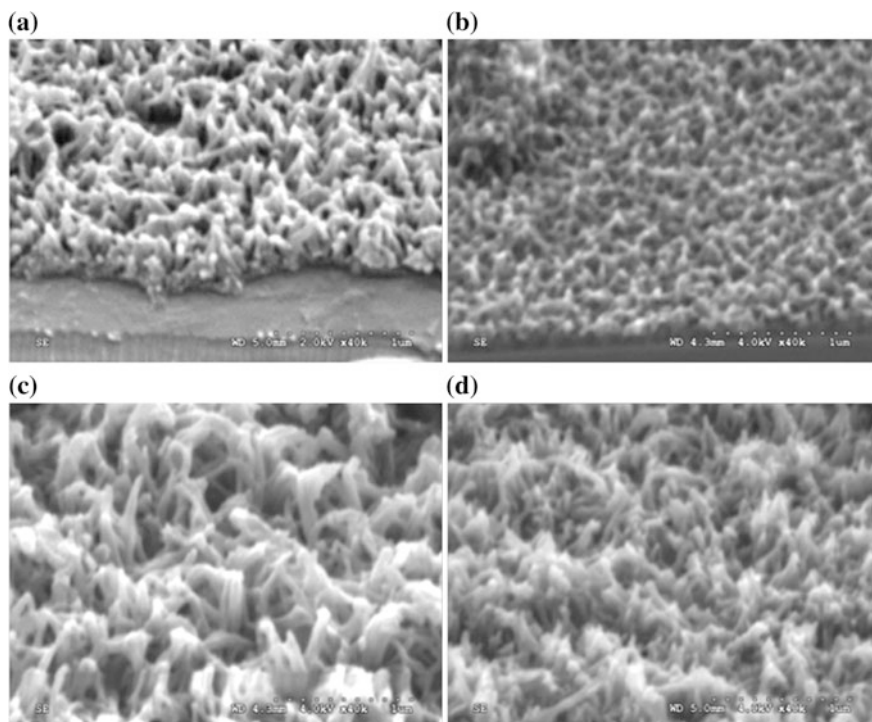


Fig. 8.8 SEM images of first layer of PANI array synthesized using different dopant: 1 M HCl (a); 2 M HCl (b); 1 M HClO₄ (c); and 2 M HClO₄ (Reproduced from Ref. [101] with kind permission of © 2013 Elsevier)

self-assemble molecule-induced dilute solution method was used for PANI arrays synthesis, then graphene paper was transferred onto it and a further PANI layer was also introduced on to graphene. In the process of synthesis, several different acids (HCl and HClO₄) were chosen as dopants. It turned out that using HClO₄ can help to achieve more favorable porous morphology and led to better electrochemical properties, which is owing to the dependence of PANI nanowire morphology on the size of dopants. At the beginning of synthesis, 4-ATP molecules were absorbed onto the gold foil and formed a soft template for ANI monomers to nucleate [102]. Subsequently, ANI monomers were in situ protonated, and the acidic radicals doped into the N atoms. Under such circumstances, the further growth can be approximately described by the dilute surfactant microcells mechanism proposed by Xia et al. [103]. Because ClO₄⁻ is much larger than Cl⁻ in size, it may generate greater steric hindrance, and thus lead to thinner nanowires. Obviously, the choice of acid in the synthesis process plays a critical role in the morphology of 3D network structures.

8.3.3 Monolayer Graphene Cross-Linked Ordered PANI

In the last synthesis method, a graphene film interconnected multilayered vertically aligned PANI nanowire array was studied. It was easy to tune the nanowire alignment and diameter to enhance the electrochemical performances by changing the dopants and their concentrations. However, two issues deteriorated their electrochemical performance more or less. First, the self-assembly small molecules between current collector and PANI hinder the charge transferring efficiency. Second, it was difficult to prepare a thin graphene interlayer by simply filtering. Hence, the densely packed graphene film significantly lowered the specific capacitance.

In the literature [104], the electrochemical deposition was employed to introduce monolayer graphene onto a PANI nanowire arrays with larger bonding strength for better charge transferring between PANI and current collector. The monolayer graphene can serve as both interlayer supporting skeleton and charge transferring media. Also, a two-step electrochemical method was used to fabricate a better aligned PANI nanowire array, in which HClO_4 was the dopant in the first step and HCl was the dopant in the second step. The role of the HClO_4 had been demonstrated to allow the PANI nucleation previously. As for HCl -doped PANI nanowires, monolayer GO can easily assembled onto the PANI nanowire array, which was proved in Fig. 8.9a, b. The whole process consists a series of intermediate reactions. First, the Cl^+ was attacked by acyl groups of carboxyl groups, and the resulted structure was an electron-defect compounds. This structure tended to bond with benzenoid amines by carbon side. Consequently, one electron was transferred from carbonyl group to acyl group, and the hypochlorite was removed from structure. Finally, the carbonyl group gave one proton away and the whole structure forms a stable amide bonding between PANI and GO.

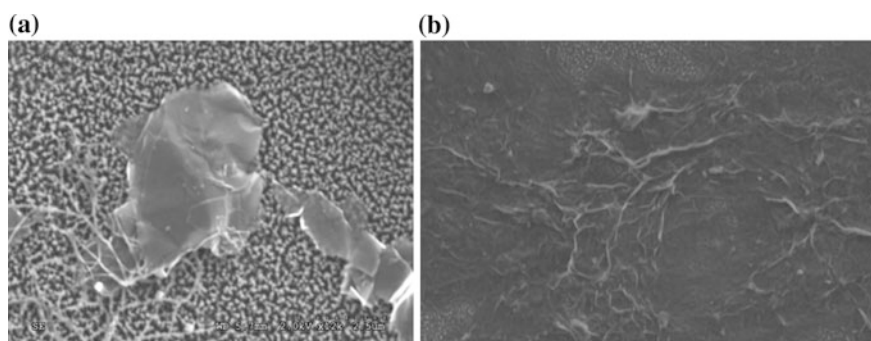


Fig. 8.9 Surface of PANI array after graphene oxide was electrochemically deposited. PANI array doped by HClO_4 (a); PANI array doped by HCl (b). Graphene oxide was deposited under 1.2 V, 5 μA for 0.5 h in both samples (Reproduced from Ref. [104] with kind permission of © 2013 Elsevier)

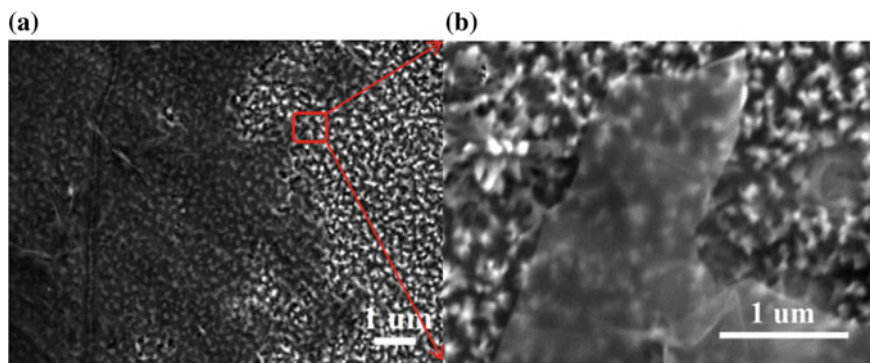


Fig. 8.10 SEM results of PANI nanowire array grown stepwise in 1 M HClO₄ for 1 h and 1 M HCl for 6 h at 2 μA/cm² current density, respectively. **a** Top view and **b** side view (Reproduced from Ref. [104] with kind permission of © 2013 Elsevier)

Therefore, a combined method was developed to produce well-aligned PANI nanowire array for readily assembly of monolayer GO. To be special, the synthesis was firstly carried out in the 1 M HClO₄ for 6 h, and then in 1 M HCl for another 1 h. Obviously, all the PANI nanowires were vertically aligned and diameter distribution was uniform, and a high coverage and continuous coating of GO was obtained and displayed in Fig. 8.10.

PANI nanowires with controlled diameter and length were vertically grown onto the GO surface while GO was in-situ reduced by an electrochemical method [105, 106]. The alternative growth of PANI nanowire array and assembly of monolayer GO was carried out for hierarchical 3D nanostructures, and the corresponding SEM results are shown in Fig. 8.11. This rationally designed architecture will be advantageous in boosting an optimal performance.

8.4 Electrochemical Performance of Polymer/Graphene Composites as Battery Electrodes

Several factors significantly affect the electrochemical performances of supercapacitor electrodes as summarized by Pandolfo and Hollenkamp in their review, such as structure of electroactive materials, electrical conductivity of electroactive materials, and the interface between electrode and electrolyte. In this chapter, hierarchical nanostructured materials consisting of stacked polymer nanowires forests interconnected by graphene sheets obtained through three synthetic methods mentioned in Sect. 8.2. After gradually improving synthetic parameter, growth of

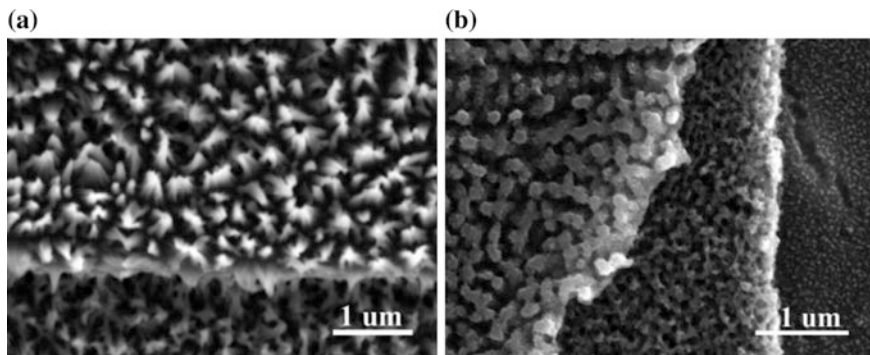


Fig. 8.11 **a** SEM image of two-stack 3D nanostructure; **b** three-stack 3D nanostructure (Reproduced from Ref. [104] with kind permission of © 2013 Elsevier)

PANI nanowire in HClO_4 and HCl stepwise is the best method for both good alignment and capability to be assembled with graphene. This structure not only can combine the high stability, high surface area, and conductivity of graphene with high capacitance of PANI. As a result, the synergistic effect between two components resulted in much superior performance. The highest specific capacitance in aqueous electrolyte was measured as 1443 F/g. Also, high energy and power density can be achieved simultaneously, specifically 100 Wh/kg at 63,534 W/kg [104].

The unique layer-dependent electrochemical performance was further investigated as shown in Fig. 8.6. For the cyclic voltammetry scanning, obvious oxidation and reduction were observed, indicating pseudo-capacitive behavior. The polarizing current increased linearly with the number of layers of the arrays. The equivalent series resistance (ESR) was less than 1.0Ω and the shape of the curve clearly indicated finite-length porous electrodes. Proton (H^+) in acid solution could significantly dope PANI and make the PANI highly conductive, thus the charge transfer happened very quickly and electrochemical behavior was primarily dependent on the diffusion process. The diffusion resistance can be approximately calculated as 0.75Ω by using equation:

$$R_{\Sigma} = 3(R_i - \text{ESR}) \quad (8.13)$$

where R_{Σ} is diffusion resistance and R_i is the intersection between high and low frequency. With the increasing number of PANI arrays, the diffusion would be more difficult because of the vertically diffusion path was blocked by GO, and thus the specific capacitance decreases slightly (Fig. 8.12).

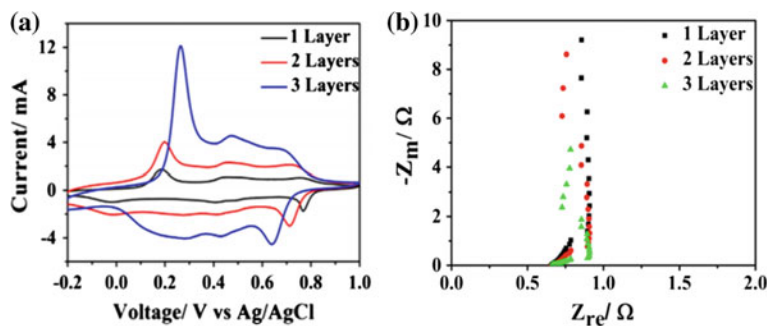


Fig. 8.12 Cyclic voltammetry of multilayered nanostructures scanned at 50 mV/s (a). Impedance test of 3D structured electrode in aqueous solutions (b) (Reproduced from Ref. [104] with kind permission of © 2013 Elsevier)

8.5 Influence of Electrolyte on Performance

Apart from advanced electrode materials, electrolyte is also a major parameter that is important in determining high-performance supercapacitors.

8.5.1 Organic Electrolytes

All the previous measurements (in Sect. 8.3) were carried out in aqueous solution. To further investigate the effect of organic electrolyte on the electrochemical behavior, the PANI/graphene composites were tested in TBAPF₆/acetonitrile electrolyte. There was no proton doping in the organic electrolyte and PANI was much less conductive, and thus charge transfer process dominates the whole electrochemical process. As shown in Fig. 8.13, the equivalent series resistance was as high as 28.1 Ω, indicating higher resistance of system. The original H⁺ doping state in first PANI nanowire array was low, conductivity was low, and thus leads to low charge transfer rate. As GO was assembled and in situ reduced, the band gap of 3D nanostructured materials was lowered, and charge carriers density was increased. With more graphene layers were introduced into the 3D nanostructures, charge transfer capability was improved. The charge transfer resistance calculated as 2, 1.7, and 0.26 Ω for one-, two- and three-layer 3D nanostructured electrodes derived from the slope of low frequency region. This also agreed well with Wang's theoretical [107].

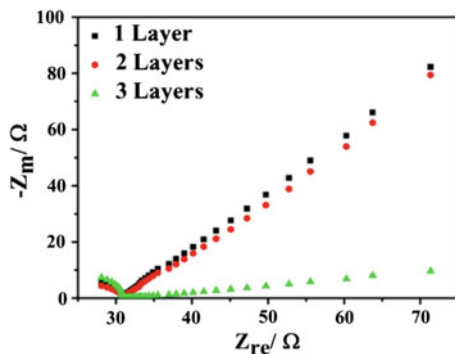


Fig. 8.13 Impedance test of 3D structured electrode in TBAPF₆/acetonitrile solutions (Reproduced from Ref. [107] with kind permission of © 2012 American Chemical Society)

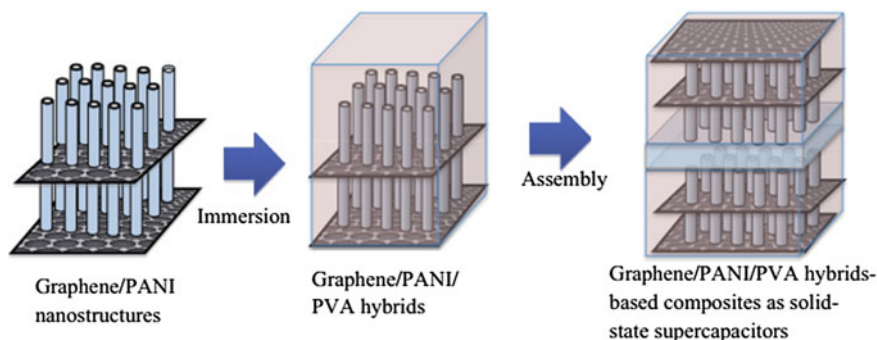


Fig. 8.14 Illustration of fabricating multiphase composites as solid-state supercapacitors. Graphene/PANI hybrid nanostructures were impregnated with PVA and assembled together to form ordered symmetrical solid-state supercapacitors (Reproduced from Ref. [108] with kind permission of © 2015 Elsevier)

8.5.2 Solid Electrolytes

Safety and relatively short cycling life are other two issues related to liquid electrolytes. Therefore, various solid-state electrolytes are suggested as promising alternatives because of their chemical and physical stability, leakage and maintenance requirements, and flexibility. Therefore, multilayered structured polyaniline (PANI) nanowire arrays linked by graphene, and then incorporated them into H₃PO₄-Nafion/PVA to form hybrid composites, which serve as solid-state supercapacitors. The relevant schematic can be seen in Fig. 8.14.

The specific capacitance was measured to be 83 F/g at 0.1 A/g, and it showed very less dependence on the current density. The hybrid composites also showed superior stability on the energy density in a big range of power density. When

power density ranged from 70 to 3600 W/kg, the energy density remained at 26.5 Wh/kg. The as-produced solid-state supercapacitors also demonstrated stable capacitance on both low frequency and high frequency, which may be due to the improved charge transporting of the solid-state electrolyte. The specific capacitance became quite stable after 13% drop in the first 400 cycles. These results indicated delicate PANI nanostructure and excellent charge transportation of the electrolyte play a critical role in the high-performance solid-state supercapacitors [108].

In order to obtain an insightful understanding of the relation between structure, electrolyte, and electrochemical performances, the electrochemical behavior was further theoretically investigated. In aqueous system, the diffusion was the dominating process since the electrochemical process was determined by the slowest step. Their electrochemical behavior can be described by the following equations [109]:

$$i_p = an^{1.5}AD^{0.5}Cv^{0.5} \quad (8.14)$$

$$i = i_p \frac{nF}{RT} (E - E_{eq}) \quad (8.15)$$

$$C_s = \frac{\int it}{\Delta Vm}, \quad (8.16)$$

where i_p stands for peak current, a is constant, 2.69×10^5 , n is number of electrons transferred, A is surface area of electrode, D is diffusion coefficient of electrolyte, v is scan rate, C is bulk concentration of electrolyte, i is electrode current, F is Faraday constant, R is gas constant, T is thermodynamic temperature, E is electrode potential, E_{eq} is equilibrium potential, C_s is specific capacitance, t is scanning time, ΔV is the voltage difference between beginning and ending scan, and m is the mass of the PANI on the electrode. Combining them together results in a new equation as follows:

$$C_s = \frac{an^{1.5}AD^{0.5}Cv^{0.5}F \int (E - E_{eq}) dt}{RT\Delta vm}. \quad (8.17)$$

Obviously, the specific capacitance was a function of sophisticated competition among number of electrons transferred; electrode surface area and electrode mass. Since PANI was in the highest doping state in aqueous solution, the number of transferred electrons versus mass would not further increased in multiple-layered electrodes. In fact, it decreased because of the forming of big nanowires. The specific electrode surface area was deteriorated as well. As a result, the specific capacitance decreased as there were more PANI nanowire arrays. On the other hand, in organic system the original H^+ doping state was low and the charge transfer was the dominated step. The GO coating played a big role in the charge transferring after its deposition and in situ reduction. Reduced GO sheets interconnected with the neighbored PANI nanowire arrays and could also tune the PANI

carries concentration, and thus increased the number of transferred electrons with increasing the layer number of 3D structures. Therefore, the electrode behaves entirely different in organic electrolyte system.

8.6 Conclusions

In summary, this chapter summarized the high efficiency approaches and the new point of view on increasing both energy density and power density by tailoring the polymer/graphene electrode architecture. Also, a theoretical model has been established to quantify the electrode structures and performance relationship and to provide the guideline for the future fabrication and optimization. Thus, it provided both experimental and theoretical approaches for constructing high energy density and high power density supercapacitors based on polymer/graphene.

References

1. Zheng X, Yan X, Sun Y et al (2015) Au-embedded ZnO/NiO hybrid with excellent electrochemical performance as advanced electrode materials for supercapacitor. *ACS Appl Mater Interfaces* 7(4):2480–2485
2. Winter M, Brodd RJ (2004) What are batteries, fuel cells, and supercapacitors? *Chem Rev* 104(10):4245–4270
3. Liu C, Yu Z et al (2010) Graphene-based supercapacitor with an ultrahigh energy density. *Nano Lett* 10(12):4863–4868
4. Prokopuk N (2004) All organic supercapacitors as alternatives to lithium batteries. Report to SERDP
5. Li L, Qin Z, Wang L et al (2010) Anchoring alpha-manganese oxide nanocrystallites on multi-walled carbon nanotubes as electrode materials for supercapacitor. *J Nanopart Res* 12:2349–2353
6. Stoller M, Park S, Zhu Y et al (2008) Graphene-based ultracapacitors. *Nano Lett* 8:3498–3502
7. Sun Y, Shi G (2013) Graphene/polymer composites for energy applications. *J Polym Sci Polym Phys* 51(4):231–253
8. Graeme A, Pon K, Adam S (2011) Conducting-polymer-based supercapacitor devices and electrodes. *J Power Sources* 196(1):1–12
9. Yoo JJ, Balakrishnan K, Huang J et al (2011) Ultrathin planar graphene supercapacitors. *Nano Lett* 11(4):1423–1427
10. El-Kady MF, Strong V, Dubin S et al (2012) Laser scribing of high-performance and flexible graphene-based electrochemical capacitors. *Science* 335(6074):1326–1330
11. Zhu Y, Murali S, Stoller MD et al (2011) Carbon-based supercapacitors produced by activation of graphene. *Science* 332(6037):1537–1541
12. Rose M, Korenblit Y, Kockrick E et al (2011) Hierarchical micro and mesoporous carbide-derived carbon as a high-performance electrode material in supercapacitors. *Small* 7(8):1108–1117
13. Izadi-Najafabadi A, Yamada T, Futaba DN et al (2011) High-power supercapacitor electrodes from single-walled carbon nanohorn/nanotube composite. *ACS Nano* 5(2):811–819

14. Korenblit Y, Kajdos A, West WC (2012) In situ studies of ion transport in microporous supercapacitor electrodes at ultralow temperatures. *Adv Funct Mater* 22(8):1655–1662
15. Pech D, Brunet M, Durou H et al (2010) Ultrahigh-power micrometre-sized supercapacitors based on onion-like carbon. *Nat Nanotechnol* 5(9):651–654
16. Liu H, Jin LH, He P et al (2009) Direct synthesis of mesoporous carbon nanowires in nanotubes using MnO_2 nanotubes as a template and their application in supercapacitors. *Chem Commun* 44:6813–6815
17. Chen Z, Augustyn V, Wen J et al (2011) High-performance supercapacitors based on intertwined CNT/ V_2O_5 nanowire nanocomposites. *Adv Mater* 23(6):791–795
18. Heywang G, Jonas F (1992) Poly(alkylenedioxythiophene) s-new, very stable conducting polymers. *Adv Mater* 4(2):116–118
19. Sivakkumar SR, Saraswathi R (2004) Performance evaluation of poly(*N*-methylaniline) and polyisothianaphthene in charge-storage devices. *J Power Sources* 137(2):322–328
20. Ryu KS, Kim KM, Park NG et al (2002) Symmetric redox supercapacitor with conducting polyaniline electrodes. *J Power Sources* 103(2):305–309
21. Talbi H, Just PE, Dao LH (2003) Electropolymerization of aniline on carbonized polyacrylonitrile aerogel electrodes: applications for supercapacitors. *J Appl Electrochem* 33(6):465–473
22. Gómez-Romero P, Chojak M, Cuentas-Gallegos K et al (2003) Hybrid organic-inorganic nanocomposite materials for application in solid state electrochemical supercapacitors. *Electrochem Commun* 5(2):149–153
23. Kulesza PJ, Skunik M, Baranowska B et al (2006) Fabrication of network films of conducting polymer-linked polyoxometallate-stabilized carbon nanostructures. *Electrochim Acta* 51(11):2373–2379
24. Hussain AMP, Kumar A, Singh F et al (2006) Effects of 160 MeV Ni^{12+} ion irradiation on HCl doped polyaniline electrode. *J Phys D Appl Phys* 39(4):750
25. Ryu KS, Lee YG, Kim KM et al (2005) Electrochemical capacitor with chemically polymerized conducting polymer based on activated carbon as hybrid electrodes. *Synth Met* 153(1):89–92
26. Khomenko V, Frackowiak E, Beguin F (2005) Determination of the specific capacitance of conducting polymer/nanotubes composite electrodes using different cell configurations. *Electrochim Acta* 50(12):2499–2506
27. Jang J, Bae J, Choi M et al (2005) Fabrication and characterization of polyaniline coated carbon nanofiber for supercapacitor. *Carbon* 43(13):2730–2736
28. Zhang J, Shan D, Mu S (2006) A rechargeable Zn- poly(aniline-*co*-*m*-aminophenol) battery. *J Power Sources* 161(1):685–691
29. Wu M, Snook GA, Gupta V et al (2005) Electrochemical fabrication and capacitance of composite films of carbon nanotubes and polyaniline. *J Mater Chem* 15(23):2297–2303
30. Ryu KS, Lee Y, Han KS et al (2004) Electrochemical supercapacitor based on polyaniline doped with lithium salt and active carbon electrodes. *Solid State Ionics* 175(1):765–768
31. Neves S, Fonseca CP (2004) Mixed solid device based on conducting polymer composite and polymer electrolyte. *J Braz Chem Soc* 15(3):395–399
32. Karami H, Mousavi MF, Shamsipur M (2003) A new design for dry polyaniline rechargeable batteries. *J Power Sources* 117(1):255–259
33. Gurunathan K, Amalnerkar DP, Trivedi DC (2003) Synthesis and characterization of conducting polymer composite (PAN/ TiO_2) for cathode material in rechargeable battery. *Mater Lett* 57(9):1642–1648
34. Ryu KS, Kim KM, Hong YG et al (2002) The polyaniline electrode doped with Li salt and protonic acid in lithium secondary battery. *Bull Korean Chem Soc* 23(8):1144–1148
35. Neves S, Fonseca CP (2002) Influence of template synthesis on the performance of polyaniline cathodes. *J Power Sources* 107(1):13–17
36. Oyama N, Hatozaki O (2000) Lithium polymer battery with high energy density. *Macromol Symp Wiley-VCH* 156(1):171–178

37. Oyama N, Hatozaki O (2000) New composite cathodes for lithium rechargeable batteries. *Mol Cryst Liquid Crystals* 349(1):329–334
38. Oyama N (2000) Development of polymer-based lithium secondary battery. *Macromol Symp Wiley-VCH* 159(1):221–228
39. Vol'fkovich YM, Bobe SL, Shlepakov AV et al (1993) Discharge macrokinetics of polyaniline electrode. *Russ Electrochem* 29(5):794–804
40. Li H, Wang J, Chu Q et al (2009) Theoretical and experimental specific capacitance of polyaniline in sulfuric acid. *J Power Sources* 190(2):578–586
41. Zhao GY, Li HL (2008) Preparation of polyaniline nanowire arrayed electrodes for electrochemical supercapacitors. *Micropor Mesopor Mater* 110(2):590–594
42. Wu Q, Xu Y, Yao Z et al (2010) Supercapacitors based on flexible graphene/polyaniline nanofiber composite films. *ACS Nano* 4(4):1963–1970
43. Hung PJ, Chang KH, Lee YF et al (2010) Ideal asymmetric supercapacitors consisting of polyaniline nanofibers and graphene nanosheets with proper complementary potential windows. *Electrochim Acta* 55(20):6015–6021
44. Snook GA, Chen GZ, Fray DJ et al (2004) Studies of deposition of and charge storage in polypyrrole-chloride and polypyrrole-carbon nanotube composites with an electrochemical quartz crystal microbalance. *J Electroanal Chem* 568:135–142
45. Snook GA, Chen GZ (2008) The measurement of specific capacitances of conducting polymers using the quartz crystal microbalance. *J Electroanal Chem* 612(1):140–146
46. Hashmi SA, Upadhyaya HM (2002) Polypyrrole and poly(3-methyl thiophene)-based solid state redox supercapacitors using ion conducting polymer electrolyte. *Solid State Ionics* 152:883–889
47. Wang J, Xu Y, Chen X et al (2007) Capacitance properties of single wall carbon nanotube/polypyrrole composite films. *Compos Sci Technol* 67(14):2981–2985
48. Wang J, Xu Y, Chen X et al (2007) Electrochemical supercapacitor electrode material based on poly(3,4-ethylenedioxythiophene)/polypyrrole composite. *J Power Sources* 163(2):1120–1125
49. Tripathi SK, Kumar A, Hashmi SA (2006) Electrochemical redox supercapacitors using PVdF-HFP based gel electrolytes and polypyrrole as conducting polymer electrode. *Solid State Ionics* 177(33):2979–2985
50. Hussain AMP, Saikia D, Singh F et al (2005) Effects of 160 MeV Ni¹²⁺ ion irradiation on polypyrrole conducting polymer electrode materials for all polymer redox supercapacitor. *Nucl Instrum Meth B* 240(4):834–841
51. Fan LZ, Maier J (2006) High-performance polypyrrole electrode materials for redox supercapacitors. *Electrochem Commun* 8(6):937–940
52. Boyano I, Bengoechea M, de Meatza I et al (2007) Improvement in the Ppy/V₂O₅ hybrid as a cathode material for Li ion batteries using PSA as an organic additive. *J Power Sources* 166(2):471–477
53. Boyano I, Bengoechea M, de Meatza I et al (2007) Influence of acids in the Ppy/V₂O₅ hybrid synthesis and performance as a cathode material. *J Power Sources* 174(2):1206–1211
54. Wang J, Wang CY, Too CO et al (2006) Highly-flexible fibre battery incorporating polypyrrole cathode and carbon nanotubes anode. *J Power Sources* 161(2):1458–1462
55. Wang CY, Ballantyne AM, Hall SB et al (2006) Functionalized polythiophene-coated textile: a new anode material for a flexible battery. *J Power Sources* 156(2):610–614
56. Sung JH, Kim SJ, Jeong SH et al (2006) Flexible micro-supercapacitors. *J Power Sources* 162(2):1467–1470
57. Hallik A, Aluma A, Tamm J et al (2006) Analysis of electrochemical impedance of polypyrrole|sulfate and polypyrrole|perchlorate films. *Synth Met* 156(5):488–494
58. Wang J, Too CO, Zhou D et al (2005) Novel electrode substrates for rechargeable lithium/polypyrrole batteries. *J Power Sources* 140(1):162–167
59. Izadi-Najafabadi A, Tan DTH, Madden JD (2005) Towards high power polypyrrole/carbon capacitors. *Synth Met* 152(1):129–132

60. Yang J, Martin DC (2004) Microporous conducting polymers on neural microelectrode arrays: II. Physical characterization. *Sensor Actuat A-Phys* 113(2):204–211
61. Xiao Q, Zhou X (2003) The study of multiwalled carbon nanotube deposited with conducting polymer for supercapacitor. *Electrochim Acta* 48(5):575–580
62. Sung JH, Kim SJ, Lee KH (2003) Fabrication of microcapacitors using conducting polymer microelectrodes. *J Power Sources* 124(1):343–350
63. Iroh JO, Levine K (2003) Capacitance of the polypyrrole/polyimide composite by electrochemical impedance spectroscopy. *J Power Sources* 117(1):267–272
64. Park JH, Ko JM, Park OO et al (2002) Capacitance properties of graphite/polypyrrole composite electrode prepared by chemical polymerization of pyrrole on graphite fiber. *J Power Sources* 105(1):20–25
65. Garcia-Belmonte G, Bisquert J (2002) Impedance analysis of galvanostatically synthesized polypyrrole films. Correlation of ionic diffusion and capacitance parameters with the electrode morphology. *Electrochim Acta* 47(26):4263–4272
66. Amanokura J, Suzuki Y, Imabayashi S et al (2001) Polypyrrole/polymer electrolyte composites prepared by in situ electropolymerization of pyrrole as cathode/electrolyte material for facile electron transfer at the solid interface. *J Electrochem Soc* 148(4):D43–D48
67. Chen GZ, Shaffer MSP, Coleby D et al (2000) Carbon nanotube and polypyrrole composites: coating and doping. *Adv Mater* 12(7):522–526
68. Suematsu S, Oura Y, Tsujimoto H et al (2000) Conducting polymer films of cross-linked structure and their QCM analysis. *Electrochim Acta* 45(22):3813–3821
69. Lota K, Khomenko V, Frackowiak E (2004) Capacitance properties of poly(3,4-ethylenedioxythiophene)/carbon nanotubes composites. *J Phys Chem Solids* 65(2):295–301
70. Wang J, Too CO, Wallace GG (2005) A highly flexible polymer fibre battery. *J Power Sources* 150:223–228
71. Park JH, Kim JH, Lee HK et al (2004) A novel direct deposition of Pt catalysts on Nafion impregnated with polypyrrole for PEMFC. *Electrochim Acta* 50(2):769–775
72. Kim BC, Ko JM, Wallace GG (2008) A novel capacitor material based on Nafion-doped polypyrrole. *J Power Sources* 177(2):665–668
73. Zhang LL, Li HH, Fan CY et al (2015) Polypyrrole nanosphere embedded in wrinkled graphene layers to obtain cross-linking network for high performance supercapacitors. *Electrochim Acta* 184:179–185
74. Gan JK, Lim YS, Huang NM et al (2015) Effect of pH on morphology and supercapacitive properties of manganese oxide/polypyrrole nanocomposite. *Appl Surf Sci* 357:479–486
75. Ru-Shi L (ed) (2012) *Controlled nanofabrication: advances and applications*. CRC Press, Boca Raton, p 508
76. Pettersson LAA, Carlsson F, Inganäs O et al (1998) Spectroscopic ellipsometry studies of the optical properties of doped poly(3,4-ethylenedioxythiophene): an anisotropic metal. *Thin Solid Films* 313:356–361
77. Czardybon A, Lapkowski M (2001) Synthesis and electropolymerisation of 3,4-ethylenedioxythiophene functionalised with alkoxy groups. *Synth Met* 119(1–3):161–162
78. Tong L, Skorenko KH, Faucett AC et al (2015) Vapor-phase polymerization of poly(3,4-ethylenedioxythiophene) (PEDOT) on commercial carbon coated aluminum foil as enhanced electrodes for supercapacitors. *J Power Sources* 297:195–201
79. Zhao Q, Wang G, Yan K et al (2015) Binder-free porous PEDOT electrodes for flexible supercapacitors. *J Appl Polym Sci* 132(41):9
80. Laforgue A (2011) All-textile flexible supercapacitors using electrospun poly(3,4-ethylenedioxythiophene) nanofibers. *J Power Sources* 196(1):559–564
81. Wagner H (2012) Influence of temperature on electrical conductivity of diluted aqueous solutions. *Power Plant Chem* 14(7):455–469

82. Usobiaga A, de Diego A, Madariaga JM (2000) Electrical conductivity of concentrated aqueous mixtures of HCl and KCl in a wide range of compositions and temperatures. *J Chem Eng Data* 45(1):23–28
83. Isono T (1984) Density, viscosity, and electrolytic conductivity of concentrated aqueous electrolyte solutions at several temperatures. Alkaline-earth chlorides, lanthanum chloride, sodium chloride, sodium nitrate, sodium bromide, potassium nitrate, potassium bromide, and cadmium nitrate. *J Chem Eng Data* 29(1):45–52
84. Wang H, Hao Q, Yang X et al (2010) Effect of graphene oxide on the properties of its composite with polyaniline. *ACS Appl Mater Interf* 2(3):821–828
85. Niedermeyer H, Hallett JP, Villar-Garcia IJ et al (2012) Mixtures of ionic liquids. *Chem Soc Rev* 41(23):7780–7802
86. MacFarlane DR, Forsyth M, Izgorodina EI et al (2009) On the concept of ionicity in ionic liquids. *Phys Chem Chem Phys* 11(25):4962–4967
87. Achuthan S, Chung BJ, Ghosh P et al (2011) A modified Stokes–Einstein equation for A β aggregation. *BMC Bioinform* 12(10):1
88. Seki S, Hayamizu K, Tsuzuki S et al (2009) Relationships between center atom species (N, P) and ionic conductivity, viscosity, density, self-diffusion coefficient of quaternary cation room-temperature ionic liquids. *Phys Chem Chem Phys* 11(18):3509–3514
89. Keskin S, Kayrak-Talay D, Akman U et al (2007) A review of ionic liquids towards supercritical fluid applications. *J Supercrit Fluid* 43(1):150–180
90. Francisco BE, Jones CM, Lee SH et al (2012) Nanostructured all-solid-state supercapacitor based on $\text{Li}_2\text{S-P}_2\text{S}_5$ glass-ceramic electrolyte. *Appl Phys Lett* 100(10):103902
91. Wang X, Hou Y, Zhu Y et al (2013) An aqueous rechargeable lithium battery using coated Li metal as anode. *Sci Rep* 3:1401
92. Chou SL, Wang YX, Xu J et al (2013) A hybrid electrolyte energy storage device with high energy and long life using lithium anode and MnO_2 nanoflake cathode. *Electrochem Commun* 31:35–38
93. Ohtomo T, Hayashi A, Tatsumisago M et al (2013) All-solid-state lithium secondary batteries using the $75\text{Li}_2\text{S-}25\text{P}_2\text{S}_5$ glass and the $70\text{Li}_2\text{S-}30\text{P}_2\text{S}_5$ glass-ceramic as solid electrolytes. *J Power Sources* 233:231–235
94. Chen PC, Shen G, Sukcharoenchoke S et al (2009) Flexible and transparent supercapacitor based on In_2O_3 nanowire/carbon nanotube heterogeneous films. *Appl Phys Lett* 94(4):043113
95. Capiglia C, Mustarelli P, Quartarone E et al (1999) Effects of nanoscale SiO_2 on the thermal and transport properties of solvent-free, poly(ethylene oxide)(PEO)-based polymer electrolytes. *Solid State Ionics* 118(1):73–79
96. Yu H, Wu J, Fan L et al (2011) Improvement of the performance for quasi-solid-state supercapacitor by using PVA–KOH–KI polymer gel electrolyte. *Electrochim Acta* 56(20):6881–6886
97. Kamaya N, Homma K, Yamakawa Y et al (2011) A lithium superionic conductor. *Nat Mater* 10(9):682–686
98. Foertig A, Baumann A, Rauh D et al (2009) Charge carrier concentration and temperature dependent recombination in polymer-fullerene solar cells. *Appl Phys Lett* 95(5):052104
99. Sproul AB, Green MA (1993) Intrinsic carrier concentration and minority-carrier mobility of silicon from 77 to 300 K. *J Appl Phys* 73(3):1214–1225
100. Li L, Qiu J, Wang S (2013) Polyaniline nanowire-pillared graphene for supercapacitor electrode. *Soft Mater* 11:503–509
101. Li L, Qiu J, Wang S (2013) Three-dimensional ordered nanostructures for supercapacitor electrode. *Electrochim Acta* 99:278–284
102. Wu J, Tang Q, Li Q, Lin J (2008) Self-assembly growth of oriented polyaniline arrays: a morphology and structure study. *Polymer* 49:5262–5267
103. MacDiarmid A, Epstein A (1995) Secondary doping in polyaniline. *Synth Met* 69:85–92
104. Li L, Zhang X, Qiu J et al (2013) Reduced graphene oxide-linked stacked polymer forests for high energy-density supercapacitor. *Nano Energy* 2(5):628–635

105. Sheng K, Sun Y, Li C et al (2012) Ultrahigh-rate supercapacitors based on electrochemically reduced graphene oxide for ac line-filtering. *Sci Rep* 2:247
106. Miller J, Outlaw R, Holloway B (2010) Graphene double-layer capacitor with ac line-filtering performance. *Science* 329:1637–1639
107. Wang R, Huang L, Tian X (2012) Understanding the protonation of polyaniline and polyaniline–graphene interaction. *J Phys Chem C* 116:13120–13126
108. Li L, Wang S, Hui D et al (2015) Ordered multiphase polymer nanocomposites for high-performance solid-state supercapacitors. *Compos Part B-Eng* 71:40–44
109. Bard AJ, Faulkner LR, Leddy J et al (1980) *Electrochemical methods: fundamentals and applications*. Wiley, New York, pp 99–231